

Structural organization, micro-phase separation and polyamorphism of liquid MgSiO_3 under compression

Luyen Thi San¹, Nguyen Van Hong^{1,2,a}, Toshiaki Iitaka², and Pham Khac Hung¹

¹ Hanoi University of Science and Technology, Hanoi, Vietnam

² Computational Astrophysics Laboratory, RIKEN, Saitama 351-0198, Japan

Received 11 September 2015 / Received in final form 6 January 2016

Published online 21 March 2016 – © EDP Sciences, Società Italiana di Fisica, Springer-Verlag 2016

Abstract. The structure, structural change and micro-phase separation in liquid MgSiO_3 under pressure are studied by molecular dynamics simulation with pair-wise potentials. Models consisting of 5000 atoms are constructed at 3500 K in the 0–30 GPa pressure range. The structural organization and structural phase transition under compression as well as network topology of liquid MgSiO_3 are clarified through analysis and visualization of molecular dynamics simulation data. The short-range structure, intermediate-range structure and the degree of polymerization as well as structural, compositional and dynamical heterogeneities are also discussed in detail.

1 Introduction

The magnesium silicate system (MgSiO_3) is an important material in many high technology applications such as refractory brick, porous ceramic membranes for catalytic reactors, dental materials. Therefore, knowledge of the microstructure of MgSiO_3 glass and melt is essential for understanding and controlling its physical and chemical properties [1–4]. This knowledge is also important for geosciences because the MgSiO_3 system is the simplest (two-component oxide) approximation to the composition of the Earth's mantle, and ultramafic and mafic liquids [5–9]. Therefore, the structural properties (local structure, medium-range structure, network structure) of MgSiO_3 glasses and melts have been investigated extensively by both experiment and simulation [4–16]. The most common techniques used in experimental investigation of the molecular structure of glasses are X-ray diffraction, nuclear magnetic resonance (NMR), Raman spectroscopy, X-ray absorption techniques (EXAFS and XANES) and vibrational spectroscopy. Among these techniques, vibrational spectroscopy is especially useful for in situ investigation at high pressures and temperatures. Meanwhile, NMR and Raman spectroscopy are techniques that are especially sensitive to the states of polymerization of silicate glasses. X-ray diffraction data showed that in MgSiO_3 at ambient pressure, Mg has six-fold coordination forming a distorted octahedral structure [5] (4 O neighbors at 2.08 Å and 2 O neighbors at 2.50 Å) or four-fold coordination forming a tetrahedral structure with a mean distance $d_{\text{Mg-O}} = 2.04$ Å [6]. By using NMR, the authors in [7,8] reveal that Mg coordination consists of both five-fold and six-fold, and that six-fold is dominant. By coupling X-ray

and neutron diffraction with a reverse Monte Carlo (RMC) simulation, Wilding and co-workers [9] have recently reported that an average coordination number of Mg in MgSiO_3 is about 4.5. However, a similar study gives a higher coordination of 5.1 [10]. Based on the diffraction data, it can be interpreted that the structure of MgSiO_3 glass is a mixture of MgO_4 and MgO_5 polyhedra, which are connected to the silicate network by corner sharing with SiO_4 tetrahedra. In the works [3,11], by using neutron diffraction, high-energy X-ray diffraction data and reverse Monte Carlo modeling, the authors have shown that the fraction of MgO_4 , MgO_5 , and MgO_6 coordination units is about 68.8%, 27.8%, and 3.4%, respectively. The high proportion of MgO_4 coordination units shows that a significant amount of Mg can act as a network former. Regarding the Mg local environment, investigation results show that Mg-O bond distances in MgO_4 coordination units are shorter than in the other units (MgO_5 and MgO_6). The average Mg-O bond distance in MgSiO_3 is between 1.924 Å (in MgO_4 units) and 2.10 Å (in MgO_6 units). In relation to the silicate network, investigation results show that the silicate network in MgSiO_3 as well as CaSiO_3 comprises mainly Q_2 units, with the remaining Si being distributed between Q_1 and Q_3 units (where Q_n is the SiO_4 units with n bridging oxygens (BO); the O that links to two Si atoms is considered BO) [4,12]. There also exist about 5% of the oxygen atoms that are not linked to any Si atoms (free oxygen). These free oxygens only link to Mg. This leads to forming Mg-rich regions (subnet of MgO_n units) and high silicate connected regions (Si-rich regions) and these are also the origin of the heterogeneity of the network structure. The existence of OT_3 (T is Si or Mg) triclusters leads to local charge-unbalancing. The OMg_3 linkage (O is linked to three Mg) leads to under-bonding and OSi_3 leads to strong overbonding.

^a e-mail: hong.nguyenvan@hust.edu.vn

For charge-balancing, most of OT_3 are Si-O-Mg₂ linkages (most of oxygen atoms tend to link to one SiO_4 and two MgO_4 tetrahedra). X-Ray Raman Scattering Study of MgSiO_3 glass under compression was also investigated in [13]. Results showed that the tricluster structure (OT_3 linkages) is formed as pressure increases. The Mg-O distance increases and the non-bridge oxygens (NBO) decrease with pressure. These lead to changes in the atomic configuration in short-to-medium range in the MgSiO_3 glass at high pressure.

Besides experimental methods, simulation is also a useful tool to investigate local environment and network structure of silicate glasses and melts especially in the case of high temperature and pressure. Investigation using a molecular dynamics simulation [14] indicated tetrahedral coordination with a Mg-O distance of 1.9–1.96 Å. However, Kubicki and Lasaga predicted that Mg resides in a distorted site, with 4.3 O atom neighbors at distance about 2 Å and two more at distance 2.2 Å [15] in agreement with a recent MD simulation that indicated distorted MgO_6 octahedra with an average Mg-O distance of 2.07 Å and an average coordination number of 5.7. Simulation results of liquid MgSiO_3 and Mg_2SiO_4 show that under compression, the Si's oxygen coordination increases from four-fold coordination at low pressure to six-fold at higher pressure. This means that there is a structural phase transition under compression [16–18]. Results also show that the number of free oxygen and oxygen with one nearest neighbor of either Si or Mg decreases whereas the number of Si or Mg with two or three nearest oxygens increases with pressure [16,19]. The lifetime of Mg-O bonds in liquid Mg_2SiO_4 is very short in comparison with the one of Si-O bond [19]. In the work [20], by molecular dynamics simulation, the authors show that in the 0–24 GPa pressure range, compression in the melt structure is taken up mostly by the change of IRO by rearrangements of the second neighbor Si-O and O-O distances. This is shown by a rearrangement in the Si-O-Si bond angle. Under compression, the Si-O-Si angle distribution is shifted to smaller angles, allowing for a more dense packing of the SiO_4 tetrahedra. Structural studies of the MgSiO_3 melt at high pressure by ab initio molecular dynamics in very recent work [21] shows that the average Si-O coordination number increases nearly linearly from 6.4 to 7.3 while the Mg-O and O-O coordination numbers are almost unchanged, indicating no signature of a first-order liquid-liquid phase transition. The calculated distribution of O-Si coordination number also shows evidence for the presence of oxygen triclusters (OSi_3 linkages). Besides the microphase separation in the liquid MgO-SiO₂ system was also shown in the work [22]. Using a molecular dynamics simulation, the authors have shown that there is no ideal mixture in liquid MgO-SiO₂ system.

Despite having been investigated for a long time by both experiment and simulation, the local structure (short-range and medium-range order), network structure, polyamorphism and microphase separation in MgSiO_3 systems are still in debate and not fully resolved. Further studies are required. In this paper, we used MD simulation

Table 1. Potential interaction parameters used in MD simulations [16,23,24].

i	j	A_{ij} (eV)	B_{ij} (Å ⁻¹)	C_{ij} (eV Å ⁶)	q
Mg	Mg	0	0	0	$q_{\text{Si}} = 2.9043$
Mg	Si	0	0	0	
Mg	O	1041.43266	3.48918	0	$q_{\text{Mg}} = 1.9104$
Si	Si	0	0	0	
Si	O	1137.02499	3.53732	0	$q_{\text{O}} = -1.6049$
O	O	2023.79522	3.73972	3.30544	

to clarify the structural organization of liquid MgSiO_3 and the structural change under compression. Specifically, network structure and microphase-separation in liquid MgSiO_3 will be investigated and discussed in detail.

2 Calculation method

A molecular dynamics simulation is carried out on MgSiO_3 models consisting of 5000 atoms (1000 Si, 3000 O and 1000 Mg atoms). The Oganov (OG) potential and the periodic boundary conditions are used to construct the models. The OG potential is a simple pair-wise potential. The interatomic potential employed accounts for Coulomb forces, Born electron repulsion, and van der Waals attractive forces, having the potential shown in equation (1):

$$\phi_{ij}(r_{ij}) = \frac{q_i q_j e^2}{4\pi\epsilon_o r_{ij}} + A_{ij} \exp(-B_{ij} r_{ij}) - \frac{C_{ij}}{r_{ij}^6} \quad (1)$$

where $\phi_{ij}(r_{ij})$ is the interatomic potential; ϵ_o is the permittivity of free space; r_{ij} is the distance between atoms i and j ; q_i , and q_j are the charges of the i th and j th atoms, respectively. The parameters are shown in Table 1. Although the OG potential is a simple pair-wise potential, it reproduces accurately the recent experimental data (structural and dynamical properties) over a wide pressure range and is widely used in many recent studies [16,23–27].

To integrate the equation of motion, the Verlet algorithm is used with a time step of 0.47 fs. The initial configuration is generated by placing all atoms randomly in a simulation box and heating it up to 6000 K to remove possible memory effects. After that the sample is cooled down to 5000, 4000, and finally to 3500 K. Next, a long relaxation has been done in the NPT ensemble (constant temperature and pressure) to produce a model at 3500 K at ambient pressure. Hereafter, the obtained model is called M0. Next we produce 6 different models of liquid MgSiO_3 by compressing model M0 to different pressures. The structural data of considered models is determined by averaging over 1000 configurations during the last 10^4 MD steps.

3 Results and discussions

To assure the reliability, the structural characteristics are calculated and compared to experimental data as well as other simulation results. The partial pair radial distribution function (PPRDF) of liquid MgSiO_3 at different pressures (ambient pressure, 15 and 30 GPa) is shown in Figure 1. It can be seen that the height of the first peak of

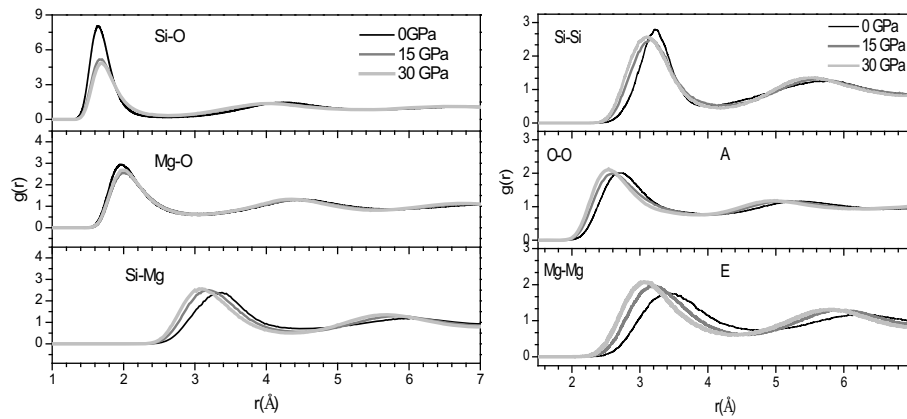


Fig. 1. Partial pair radial distribution function $g_{\text{Si-O}}(r)$, $g_{\text{Mg-O}}(r)$, $g_{\text{Si-Mg}}(r)$, $g_{\text{Si-Si}}(r)$, $g_{\text{O-O}}(r)$ and $g_{\text{Mg-Mg}}(r)$ of liquid MgSiO_3 at different pressures.

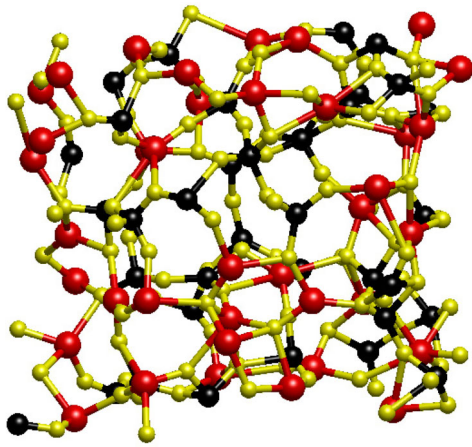


Fig. 2. Network structure of MgSiO_3 at ambient pressure, where the large red sphere is Mg, the black sphere is Si, and the small yellow sphere is O.

PPRDF $g_{\text{Si-O}}(r)$ and $g_{\text{Mg-O}}(r)$ is significantly changed in the 0–15 GPa pressure range but in the 15–30 GPa pressure range, it is almost unchanged. In the considered pressure range, the position of first peak of PPRDFs $g_{\text{Si-O}}(r)$ and $g_{\text{Mg-O}}(r)$ increases very slightly as pressure increases. The position of the first peak of Si-O PPRDF at 0, 15 and 30 GPa is at 1.64, 1.66 and 1.68 Å, respectively. For Mg-O PPRDF, at 0, 15 and 20 GPa the first peak is located at 1.98, 2.0 and 2.02 Å, respectively, the results are in good agreement with experimental data as well as simulation results in works [4,5,19,20]. These results also show that the Si-O and Mg-O bond lengths are slightly changed with increasing pressure. The PPRDFs $g_{\text{Si-O}}(r)$ and $g_{\text{Mg-O}}(r)$ relate to short range order (SRO), these demonstrate that the SRO is not very sensitive to compression. The PPRDFs $g_{\text{Si-Mg}}(r)$, $g_{\text{Si-Si}}(r)$, $g_{\text{O-O}}(r)$ and $g_{\text{Mg-Mg}}(r)$ relate to intermediate range order (IRO), it can be seen that the PPRDFs $g_{\text{Si-Mg}}(r)$, $g_{\text{Si-Si}}(r)$, $g_{\text{O-O}}(r)$ and $g_{\text{Mg-Mg}}(r)$ are significantly dependent on pressure. These demonstrate that IRO is significantly changed under compression [13,20,28]. Figure 2 shows the network structure of liquid MgSiO_3 at ambient pressure, it can be seen that

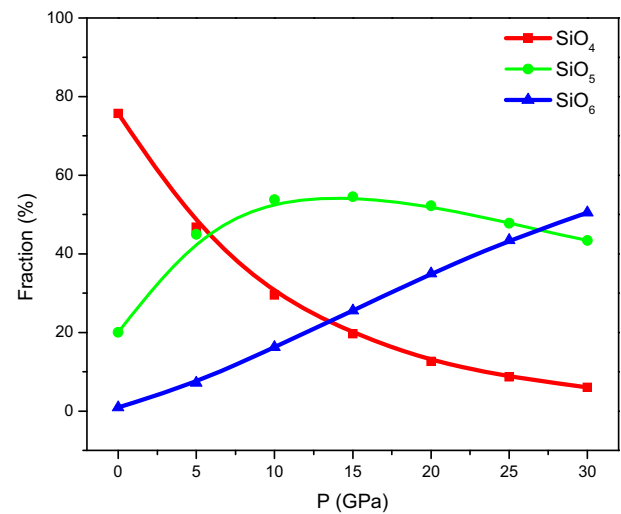


Fig. 3. Distribution of basic structural units SiO_x ($x = 4, 5, 6$) in liquid MgSiO_3 as a function of pressure.

the network structure comprises of SiO_x and MgO_n units (at ambient pressure, most of the SiO_x units are SiO_4 , most of the MgO_n units are MgO_3 , MgO_4 and MgO_5) linked to each other via one common oxygen (corner sharing) or two common oxygens (edge sharing). Figure 3 shows the pressure dependence of the fraction of basic structural units SiO_x , [coordination units or basic structural units SiO_x ($x = 4, 5, 6$) means that the Si atom is surrounded by x O atoms at the nearest neighbor distance]. Result shows that at ambient pressure, most of the basic structural units are SiO_4 and SiO_5 . The fraction of SiO_4 and SiO_5 units is about 76% and 21%, respectively. As pressure increases, the fraction of SiO_4 decreases while the fraction of SiO_5 and SiO_6 increases. At 30 GPa, most of basic structural units are SiO_5 and SiO_6 . The fraction of SiO_4 , SiO_5 and SiO_6 at 30 GPa is about 6%, 43% and 51%, respectively. Regarding the SiO_5 units we observe a maximum ($\sim 54\%$) at a pressure of around 15 GPa. It can be seen that under compression, the Si-O network structure in liquid MgSiO_3 transforms gradually from a tetrahedral to octahedral network structure [4,11]. To clarify the affect of pressure to the topology structure

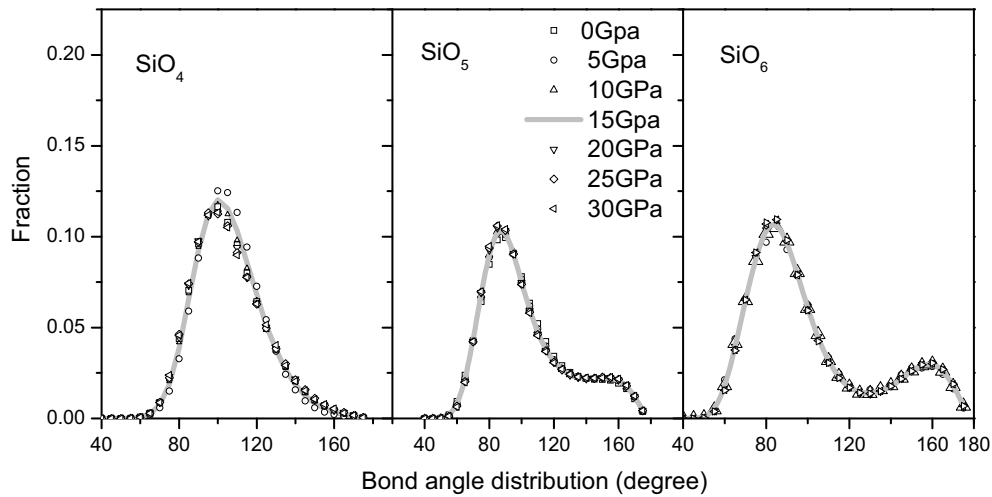


Fig. 4. The O-Si-O bond angle distribution in SiO_x ($x = 4, 5, 6$) in liquid MgSiO_3 .

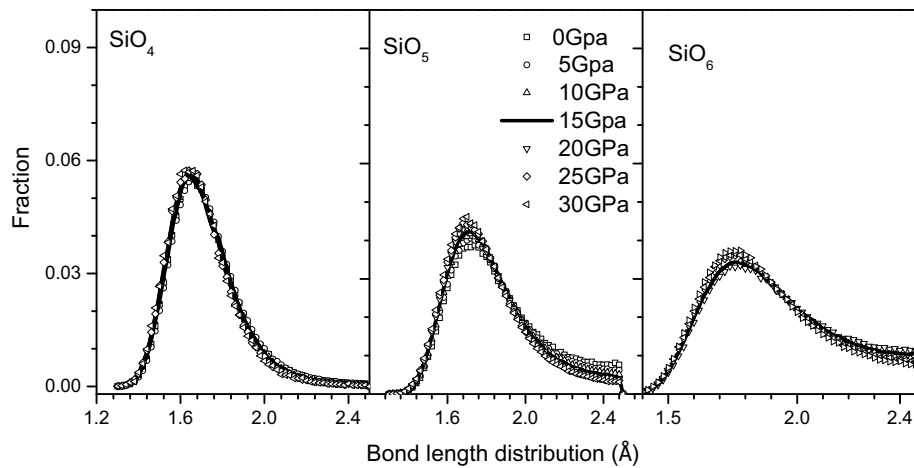


Fig. 5. Bond Si-O length distribution in SiO_x units in liquid MgSiO_3 at different pressure.

of SiO_x units, we have investigated the O-Si-O bond-angle and Si-O bond-length distribution in SiO_x units at different pressure. Figure 4 shows the O-Si-O bond angle distribution in SiO_4 , SiO_5 and SiO_6 units. It can be seen that the O-Si-O bond-angle distribution in SiO_4 , SiO_5 and SiO_6 units is not depend on compression. This means that the bond angle in SiO_x at different presures/densities is identical. The O-Si-O bond-angle distribution in SiO_4 has a pronounced peak at about 105° . For the SiO_5 , O-Si-O bond-angle distribution has a main peak at about 90° and a shoulder at 160° . For SiO_6 , the O-Si-O bond-angle distribution has a main peak at about 85° and a small peak at 160° . It can be seen that the O-Si-O bond-angle distribution in SiO_x in liquid MgSiO_3 is similar to the one in pure silica [29]. The Si-O bond-length distribution in SiO_x units is displayed in Figure 5. The result shows that the Si-O bond-length distribution in SiO_4 , SiO_5 and SiO_6 units is also not dependent on compression. The bond-length distributions in SiO_4 , SiO_5 and SiO_6 units have peaks at 1.64, 1.68 and 1.74 Å, respectively. This means that most of Si-O bond-lengths in SiO_4 , SiO_5 and SiO_6 units are about 1.64, 1.68 and 1.74 Å, respectively. The Si-O bond

distance in MgSiO_3 is a little longer in comparison to the one in pure silica [30]. The above analysis reveals that the shape and size of SiO_x units in liquid MgSiO_3 at different pressures are identical, similar to SiO_x units in liquid silica [29]. Figure 6 shows the distribution of MgO_n coordination units (left) and the distribution of average Mg-O coordination number (right) as a function of pressure. It can be seen that at low pressure, most of the MgO_n units are MgO_3 , MgO_4 and MgO_5 . At ambient pressure, the fraction of MgO_3 , MgO_4 and MgO_5 coordination units are 18%, 42% and 30%, respectively. As pressure increases, the fraction of MgO_3 and MgO_4 coordination units decreases while the fraction of MgO_n ($x = 5-9$) coordination units increases. The fraction of MgO_5 increases to a maximum ($\sim 41\%$) at about 5 GPa then decreases. The fraction of MgO_6 increases to maximum ($\sim 40\%$) at about 15 GPa then decreases gradually. At high pressure, most of MgO_n coordination units are MgO_6 , MgO_7 and MgO_8 . At 30 GPa, the fraction of MgO_6 , MgO_7 and MgO_8 is about 30%, 39% and 19%, respectively. This result shows that the local structure of Mg atoms in MgSiO_3 is significantly dependent on compression [16,17]. To clarify the

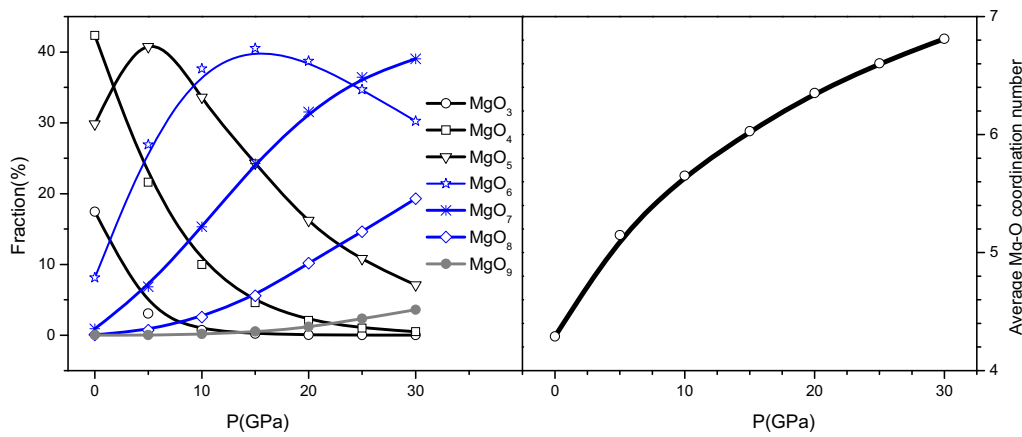


Fig. 6. Distribution of MgO_x coordination units (left) and average Mg-O coordination number (right).

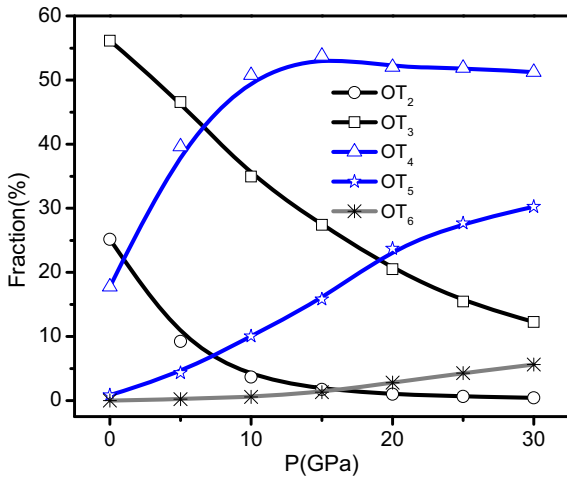


Fig. 7. Distribution of linkages OT_y ($y = 2-6$; T is Si or Mg) as a function of pressure.

IRO structure of liquid MgSiO₃, the characteristics of all type of OT_y ($T = \text{Si, Mg}$; $y = 2-6$) linkages has been investigated in detail. Figure 7 shows the distribution of OT_y linkages in liquid MgSiO₃. At low pressure (below 5 GPa), most of the linkages are OT₂, OT₃ and OT₄. At ambient pressure, the fraction of OT₂, OT₃ and OT₄ linkage is 25%, 56% and 18%, respectively. The fraction of OT₅ and OT₆ linkages is very small (about 1%). As pressure increases, the fraction of OT₂ and OT₃ linkages decreases; meanwhile the fraction of OT₄ and OT₅ and OT₆ linkages increases. At high pressure (beyond 10 GPa), most of the linkages are OT₃, OT₄ and OT₅. At pressure of 30 GPa, the fraction of OT₃, OT₄ and OT₅ is about 12%, 51% and 30%, respectively. The fraction of other linkages (OT₂ and OT₆) is very small. Figure 8 shows the distribution of the fraction of oxygen atoms forming types of OT_y linkages in liquid MgSiO₃ at different pressures. This result shows that most of the oxygen atoms form OT₂ and OT₃ linkages (at low pressure) and OT₄ and OT₅ linkages (at high pressure). It can be seen that most of the OT₂ linkages are Si-O-Mg and Si-O-Si. At ambient pressure, the fraction of Si-O-Mg and Si-O-Si linkages

is about 11% and 13%, respectively. The fraction of O-Mg₂ linkages is very small (below 1%). For OT₃ linkages, most of them are Mg-O-Si₂ and Mg₂-O-Si. The fraction of O-Mg₃ and O-Si₃ is very small. At ambient pressure, the fraction of Mg-O-Si₂, Mg₂-O-Si, O-Mg₃ and O-Si₃ linkages is about 22%, 27%, 4% and 2%, respectively. The fraction of O-Si₃ depends slightly on pressure while the fraction of other ones decreases strongly with increasing pressure. At 30 GPa, the fraction of Mg-O-Si₂, Mg₂-O-Si and O-Si₃ linkages is about 7%, 3% and 2.5%. The fraction of O-Mg₃ is below 1% at pressure beyond 10 GPa. Regarding OT₄ linkages in the considered pressure range, it can be seen that most of them are Mg₃-O-Si, Mg-O-Si₃ and Si₂-O-Mg₂. At ambient pressure, the fraction of Mg₃-O-Si and Si₂-O-Mg₂ is about 8% and 6%, respectively. The fraction of other linkages is very small, below 3%. As pressure increases, the fraction of O-Mg₄ decreases while the other ones increase. The fraction of Mg₃-O-Si linkages increases with pressure and reaches a maximum (about 18%) at 10 GPa. The fraction of Mg₂-O-Si₂ linkages increases with pressure and reaches a maximum (about 26%) at 15 GPa, then it decreases. At 30 GPa, the fraction of Mg₃-O-Si, Mg-O-Si₃ and Si₂-O-Mg₂ is 14%, 10% and 23%, respectively. For OT₅ linkages, most of them are Mg₃-O-Si₂, Mg₄-O-Si and Mg₂-O-Si₃ and they increase with pressure. The fraction of O-Mg₅, O-Si₅ and Mg-O-Si₄ linkages is very small (below 3%) [16]. The above analysis shows that most of the O atoms link to two or three Si atoms forming an Si-O network. This means that Si is the network former and Mg atoms act as both network-former and network modifier [4,11]. Due to the existence of Mg atoms (network modifier), the Si-O network in MgSiO₃ is broken into subnets, see Figure 9. The Mg atoms incorporate in Si-O subnet. The Mg atoms tend to incorporate into the Si-O subnet via both non-bridging and bridging oxygens forming Mg-O-Si, Mg₂-O-Si, Mg₃-O-Si, Mg₄-O-Si, Mg-O-Si₂, Mg₂-O-Si₂, Mg₃-O-Si₂, Mg-O-Si₃ and Mg₂-O-Si₃ linkages, see Figure 10. It also exists a number of free oxygens in liquid MgSiO₃ and Mg atoms tend to link with these free oxygens forming O-Mg_y ($y = 2-5$) linkages [4,12].

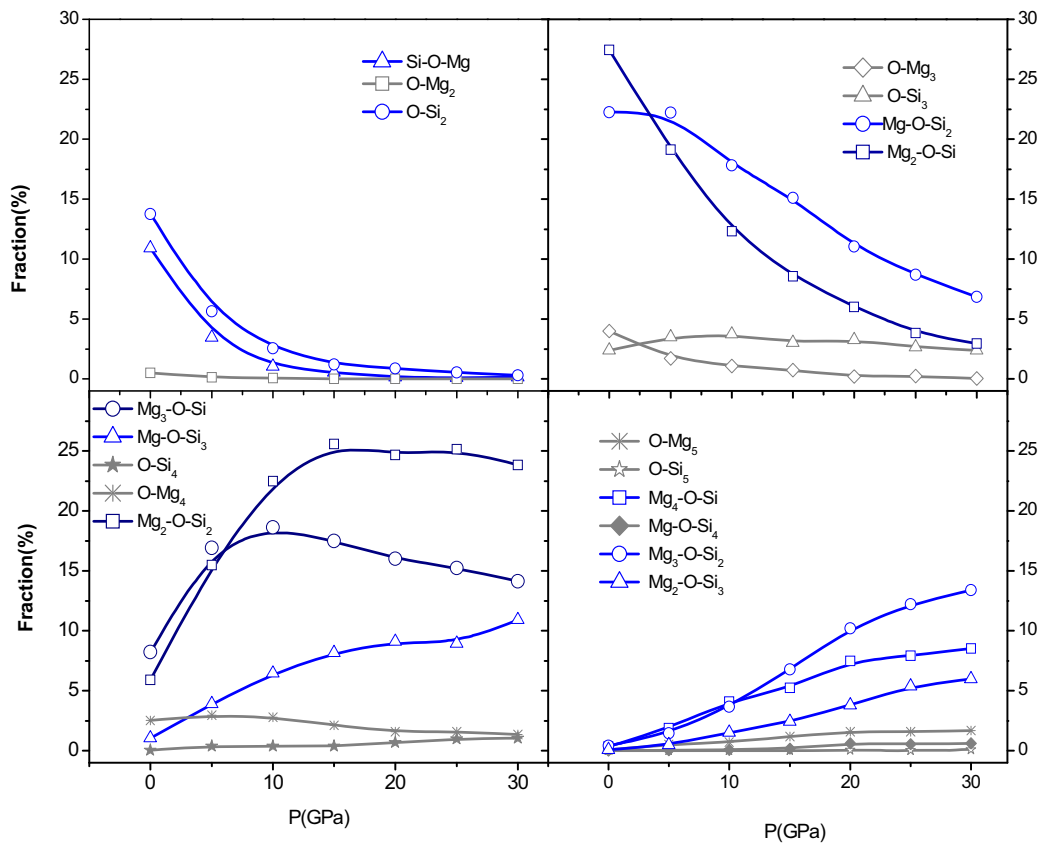


Fig. 8. Distribution of fraction of oxygen atoms forming types of linkages in MgSiO_3 as a function of pressure.

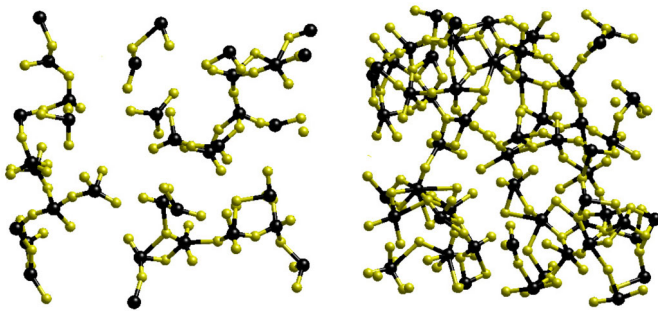


Fig. 9. The Si-O network in MgSiO_3 is broken into subnets: the figure on the left is at ambient pressure; the figure on the right is at 30 GPa, (the black sphere is the Si atom, the small yellow sphere is the O atom).

Figure 11 shows the distribution of bridging, non-bridging and free oxygens in liquid MgSiO_3 . It can be seen that at ambient pressure the fraction of bridging, non-bridging and free oxygens is about 46% and 47% and 7%, respectively. The fraction of bridging oxygens increases with pressure while the others decrease with pressure [16,19,22]. At 30 GPa, the fraction of bridging, non-bridging and free oxygens is about 69%, 27% and 4%, respectively. Details of the distribution of bridging oxygens in SiO_x units are shown in Tables 2–4. From Table 2, it can be seen that at ambient pressure the number of SiO_4

Table 2. Distribution of bridging oxygen atoms in SiO_4 units at different pressures.

P (GPa)	SiO_4	SiO_{4-0}	SiO_{4-1}	SiO_{4-2}	SiO_{4-3}	SiO_{4-4}
0	719	9	85	256	255	114
5	479	10	43	132	190	104
10	271	2	24	72	107	66
15	184	1	11	39	80	53
20	110	1	4	27	46	32
25	78	0	4	13	27	34
30	61	1	1	8	30	21

Table 3. Distribution of bridging oxygen atoms in SiO_5 units at different pressures.

P (GPa)	SiO_5	SiO_{5-0}	SiO_{5-1}	SiO_{5-2}	SiO_{5-3}	SiO_{5-4}	SiO_{5-5}
0	226	0	4	30	64	84	44
5	441	0	12	58	89	183	99
10	562	1	10	37	125	220	169
15	541	0	4	28	125	210	174
20	510	0	5	24	102	199	180
25	467	2	2	15	84	191	173
30	414	0	0	16	79	175	144

units is about 719. In these SiO_4 units there are 9 isolated SiO_{4-0} units, 85 SiO_{4-1} units, 256 SiO_{4-2} units, 255 SiO_{4-3} units, 114 SiO_{4-4} units (the SiO_4 unit with n bridging oxygens is defined as SiO_{4-n}). Results also show that most of the SiO_4 have two and three bridging oxygens.

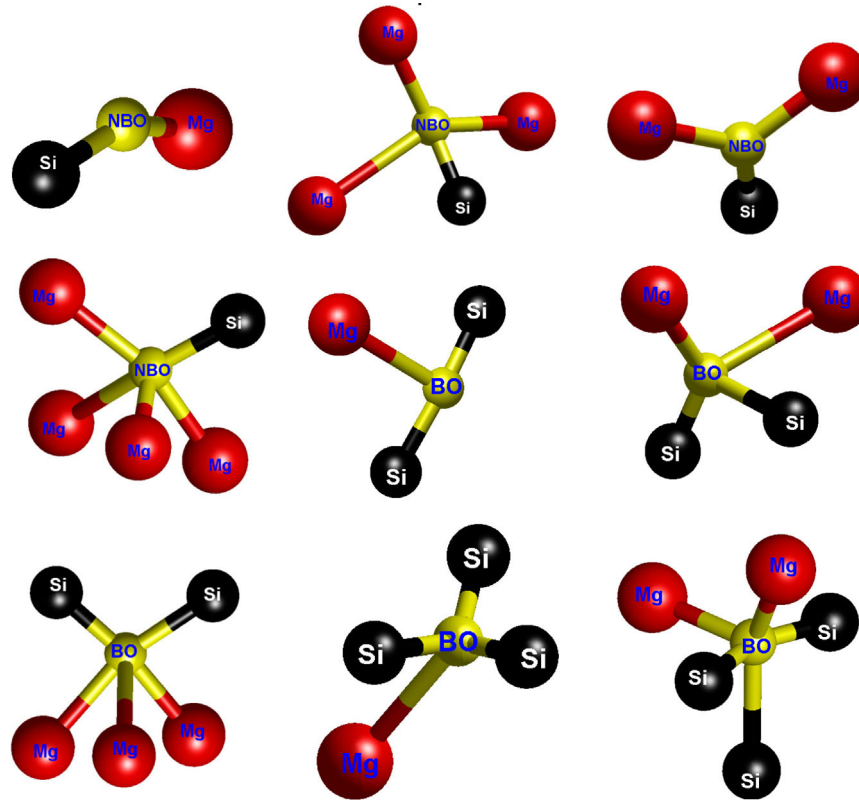


Fig. 10. Some of the main type of linkages formed by incorporation of Mg into Si-O network via bridge and non-bridge oxygens (BO and NBO).

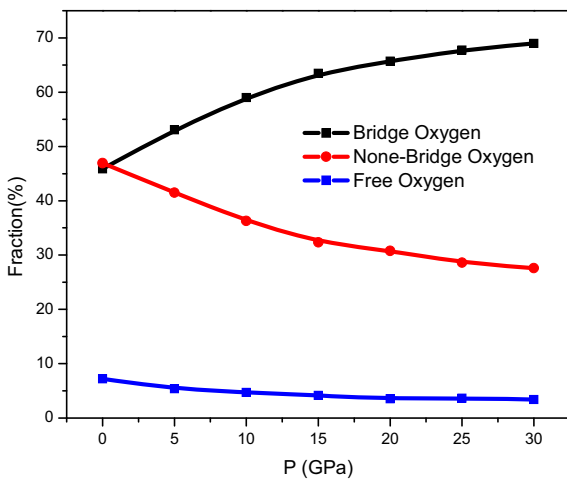


Fig. 11. Distribution of bridge, non-bridge and free oxygens in liquid MgSiO₃ as a function of pressure.

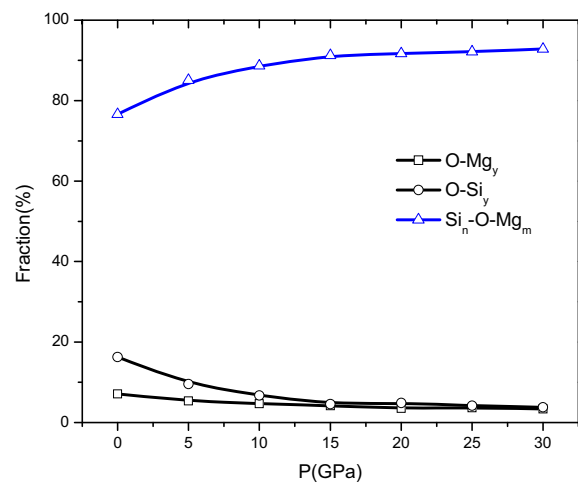


Fig. 12. Distribution of O-Si_y, O-Mg_y and Si_n-O-Mg_m linkages ($y, n, m = 1-6$) in liquid MgSiO₃ as a function of pressure. OSi_y means that O atoms only link to Si atoms. O-Mg_y means that O atoms only link to Mg atoms. Si_n-O-Mg_m means that O atoms link to both Si and Mg atoms.

Similarly, Tables 3 and 4 show the distribution of bridging oxygens in SiO₅ and SiO₆ units. Most of the SiO₅ units have three, four or five bridging oxygens. Most of the SiO₆ units have five or six bridging oxygens. Results also show that the fraction of isolated SiO_x is very small (below 1%) and only exists at low pressure. The fraction of bridging oxygens increases with pressure meaning that the degree of polymerization of the Si-O network increases with pressure and the Si-O subnets tend to incorporate

with each other, forming larger tree-shaped networks instead of isolated subnets (see Fig. 9). At low pressure, the Si-O subnets are chains of SiO_x. However, at high pressure they are clusters of SiO_x as shown in Figure 9. Figure 12 shows the distribution of O-Si_y, O-Mg_y and

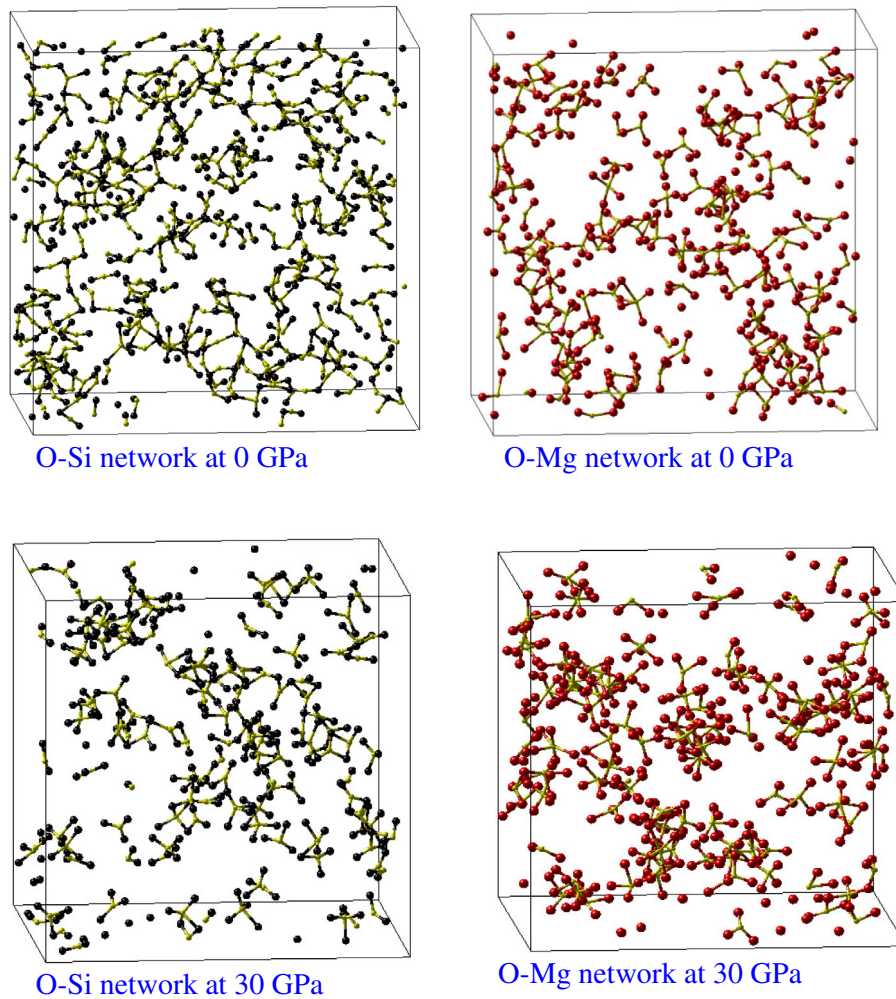


Fig. 13. Spatial distribution of O-Mg_y and O-Si_y linkages in models of liquid MgSiO₃ at different pressures. The O-Mg linkage means O atoms only bind to Mg atoms. Similarly, the O-Si linkage means O atoms only bind to Si atoms. Here, the largest red sphere is the Mg atom, the black sphere is the Si atom, the small yellow sphere is the O atom.

Table 4. Distribution of bridging oxygen atoms in SiO₆ units at different pressures.

$P(\text{GPa})$	SiO ₆	SiO ₆₋₀	SiO ₆₋₁	SiO ₆₋₂	SiO ₆₋₃	SiO ₆₋₄	SiO ₆₋₅	SiO ₆₋₆
0	13	0	0	0	1	2	6	4
5	71	0	1	1	5	10	31	23
10	160	0	0	3	20	23	55	59
15	262	0	0	4	21	42	97	98
20	359	0	1	5	21	59	139	134
25	434	0	0	4	19	73	171	167
30	474	0	2	4	26	71	173	198

Si_n-O-Mg_m linkages as a function of pressure. It can be seen that at ambient pressure, the fraction of O-Si_y, O-Mg_y and Si_n-O-Mg_m linkages is about 16%, 7% and 77%, respectively. The fraction of Si_n-O-Mg_m linkages increases with pressure while the fraction of others (O-Si_y, O-Mg_y linkages) decreases with pressure. At 30 GPa, the fraction of O-Si_y, O-Mg_y and Si_n-O-Mg_m linkages is about

4%, 4% and 92%, respectively. The spatial distribution of O-Si_y, O-Mg_y linkages is shown in Figure 13. It can be seen that the distribution of O-Si_y and O-Mg_y linkages is not uniform but that they tend to link to each other forming O-Si and O-Mg sub-networks respectively. At low pressure, both O-Mg and O-Si sub-network have the form of tree- or chain-shapes (tending to expand whole space of model) while at high pressure they have the form of cluster-shapes (tending to form isolated clusters). The above analysis demonstrates that in liquid MgSiO₃, there are heterogeneities in both structure and composition. From Figures 12 and 13, it can be seen that in liquid MgSiO₃ there exist Si-rich regions and Mg-rich regions. This means that there is a liquid-liquid micro-phase separation in liquid MgSiO₃. In other words, there is immiscibility in liquid MgSiO₃ (immiscible liquid) [20]. Figure 14 shows the network structure of liquid MgSiO₃ at low and high pressures. It can be seen that the network structure of liquid MgSiO₃ comprises chains/clusters of SiO_x units forming the main network structure. Mg atoms tend to

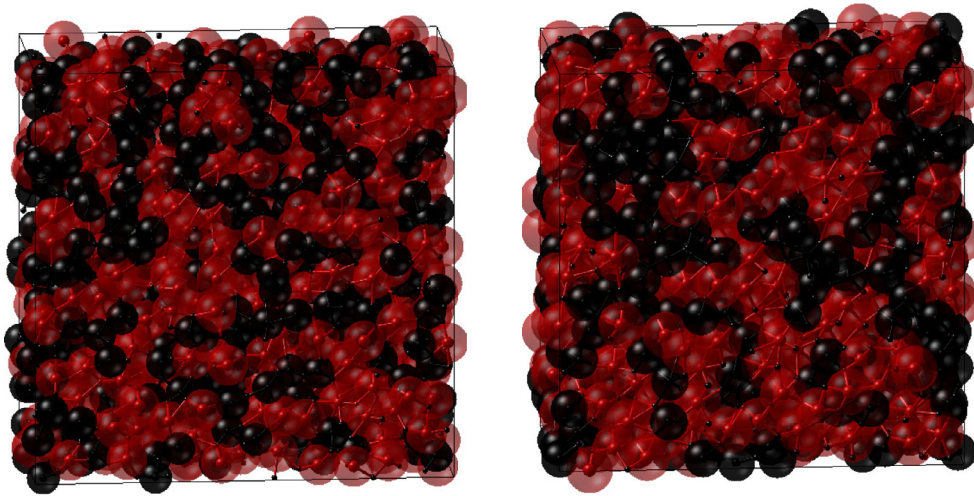


Fig. 14. Network structure of liquid MgSiO_3 at ambient pressure (left) and at 30 GPa (right). The clusters/chains of SiO_x are highlighted with black; The clusters/chains of MgO_n are highlighted with red (the units SiO_x and MgO_n are highlighted by large semi-transparent sphere).

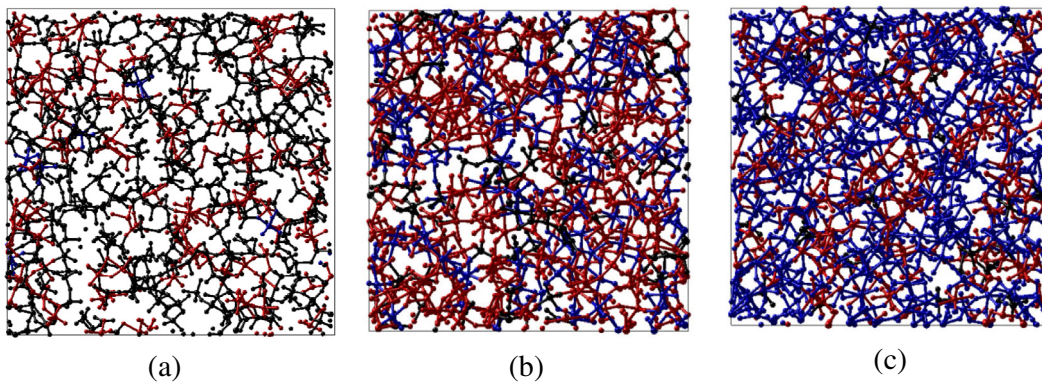


Fig. 15. The network structure of SiO_x units that are extracted from liquid MgSiO_3 at ambient pressure (a), at 15 GPa (b) and at 30 GPa (c). Clusters of SiO_4 , SiO_5 and SiO_6 are black, red and blue, respectively.

bind with free oxygen and/or non-bridging oxygen atoms forming MgO_n units that incorporate into SiO_x -chain. Chains/clusters of SiO_x form Si-rich regions. MgO_n tend to cluster forming Mg-rich regions. This is the origin of compositional and structural heterogeneities. In MgO-SiO_2 systems, the Si-O bonds are more stable than Mg-O bonds and the SiO_4 units are more stable than SiO_5 and SiO_6 units [19,30]. Therefore structural and compositional heterogeneities also lead to dynamical heterogeneity. Figure 15 shows the network of SiO_x that is extracted from liquid MgSiO_3 at different pressures. It can be seen that the network structure comprises SiO_4 , SiO_5 and SiO_6 . As shown in Figure 2, most of the basic structural units are SiO_4 (at low pressure) and SiO_5 and SiO_6 at high pressure. Under compression, there is a structural transition from SiO_4 to SiO_6 units via SiO_5 . From Figure 15, it can be seen that distribution of SiO_4 , SiO_5 and SiO_6 is not uniform but that they tend to form clusters of SiO_4 (this is highlighted in black), SiO_5 (this is highlighted in red) and SiO_6 (this is highlighted in blue) [30,31]. This is the origin of polymorphism in liquid MgSiO_3 .

4 Conclusion

Structural organization of liquid MgSiO_3 consists of SiO_x ($x = 4-6$) and MgO_n ($n = 3-9$) units. At low pressure most of the SiO_x units are SiO_4 . These SiO_x units are linked to each other via BO forming a Si-O network. At low pressure, the Si-O network is broken into subnets with a lot of NBO and Mg atoms incorporated into the Si-O network mainly via NBO forming Mg-O-Si, $\text{Mg}_2\text{-O-Si}$ and $\text{Mg}_3\text{-O-Si}$ linkages. At high pressure, the number of NBOs decrease, the Si-O network tends to extend through the whole model (the number of Si-O subnetworks decrease) and Mg atoms incorporate into the Si-O network via both BO and NBO forming $\text{Mg}_3\text{-O-Si}$, $\text{Mg}_4\text{-O-Si}$, Mg-O-Si_2 , $\text{Mg}_2\text{-O-Si}_2$, $\text{Mg}_3\text{-O-Si}_2$, Mg-O-Si_3 , $\text{Mg}_2\text{-O-Si}_3$ linkages. There also exists a small fraction of free oxygens and Mg atoms linked to free oxygens forming O-Mg_y ($y = 2-5$) linkages. These O-Mg_y linkages are not uniformly distributed in the model but they tend to form clusters of O-Mg_y . This results in Mg-rich regions. There is also a small fraction of oxygen atoms that are only linked to Si

atoms forming O-Si_y ($y = 2-5$) linkages. These O-Si_y linkages also tend to cluster forming Si-rich regions. This is the origin of microphase-separation and is evidence of compositional heterogeneity. As pressure increases, the fraction of SiO₄ decreases while the fraction of SiO₅ and SiO₆ increases. The fraction of SiO₅ reaches maximum value (54%) at pressure about 15 GPa. The size and shape of SiO₄, SiO₅ and SiO₆ units are not dependent on compression. The distribution of SiO_x units is not uniform, but there is a tendency to form clusters of SiO₄, SiO₅, SiO₆. This results in structural heterogeneity and is the origin of polymorphism. The heterogeneity of structure and composition is the cause of dynamical heterogeneity.

This research is funded by the Vietnam National Foundation for Science and Technology Development (NAFOSTED) under Grant No. 103.05-2014.40, RIKEN iTHES Project and KAKENHI (No. 26106006) from MEXT of Japan.

References

1. G. Mountjoy, B.M. Al-Hasni, Ch. Storey, *J. Non-Cryst. Solids* **357**, 2522 (2011)
2. A. Pedone, G. Malavasi, M.C. Menziani, U. Segre, A.N. Cormack, *J. Phys. Chem. C* **112**, 11034 (2008)
3. C.-C. Lina, S.-F. Chenb, L.-G. Liua, C.-C. Lia, *J. Non-Cryst. Solids* **353**, 413 (2007)
4. L. Cormier, G.J. Cuello, *Phys. Rev. B* **83**, 224204 (2011)
5. M.C. Wilding, C.J. Benmore, J.A. Tangeman, S. Sampath, *Europhys. Lett.* **67**, 212 (2004)
6. T. Taniguchi, M. Okuno, T. Matsumoto, *J. Non-Cryst. Solids* **211**, 56 (1997)
7. S. Kohara, J. Akola, H. Morita, K. Suzuya, J.K.R. Weber, M.C. Wilding, C.J. Benmore, *Proc. Natl. Acad. Sci.* **108**, 14780 (2011)
8. C.J. Benmore, E. Soignard, M. Guthrie, S.A. Amin, J.K.R. Weber, K. McKiernan, M.C. Wilding, J.L. Yarger, *J. Non-Cryst. Solids* **357**, 2632 (2011)
9. M.C. Wilding, C.J. Benmore, J.A. Tangeman, S. Sampath, *Chem. Geol.* **213**, 281 (2004)
10. M. Guignard, L. Cormier, *Chem. Geol.* **256**, 111 (2008)
11. M.C. Wilding, C.J. Benmore, J.K.R. Weber, *J. Mater. Sci.* **43**, 4707 (2008)
12. P. Zhang, P.J. Grandinetti, *Phys. Chem. B* **101**, 4004 (1997)
13. S.K. Lee, *Proc. Natl. Acad. Sci. USA* **105**, 725 (2008)
14. Yoshito Matsui, Katsuyuki Kawamura, *Nature* **285**, 648 (1980)
15. J.D. Kubicki, A.C. Lasaga, *Phys. Chem. Miner.* **17**, 661 (1991)
16. F.J. Spera, M.S. Ghiorso, D. Nevins, *Geochim. Cosmochim. Acta* **75**, 1272 (2011)
17. G. Ben Martin, F.J. Spera, M.S. Ghiorso, N. Nevins, *Am. Mineralogist* **94**, 693 (2009)
18. S.L. Chaplot, N. Choudhury, *Am. Mineralogist* **86**, 752 (2001)
19. N.P. de Koker, L. Stixrude, B.B. Karki, *Geochim. Cosmochim. Acta* **72**, 1427 (2008)
20. O. Adjaoud, G. Steinle-Neumann, S. Jahn, *Chem. Geol.* **256**, 185 (2008)
21. G. Zhao, H.F. Mu, X.M. Tan, D.H. Wang, C.L. Yang, *J. Non-Cryst. Solids* **385**, 169 (2014)
22. D.J. Lacks, D.B. Rear, J.A. Van Orman, *Geochim. Cosmochim. Acta* **71**, 1312 (2007)
23. D. Nevins, F.J. Spera, M.S. Ghiorso, *Am. Mineralogist* **94**, 975 (2009)
24. A.R. Oganov, J.P. Brodholt, G. David Price, *Phys. Earth Planet. Int.* **122**, 277 (2000)
25. Z.-J. Liu, C.-R. Zhang, X.-W. Sun, J.-B. Hu, T. Song, Y.-D. Chu, *Phys. Scr.* **83**, 045602 (2011)
26. A.M. Goryaeva, P. Carrez, P. Cordier, *Phys. Chem. Miner.* **42**, 793 (2015)
27. Z.-J. Liu, X.-W. Sun, X.-M. Tan, Y.-D. Guo, X.-D. Yang, *Solid State Commun.* **144**, 264 (2007)
28. S.J. Gaudio, S. Sen, C.E. Leshner, *Geochim. Cosmochim. Acta* **72**, 1222 (2008)
29. N.V. Hong, N.V. Huy, P.K. Hung, *Int. J. Comput. Mater. Sci. Surf. Eng.* **5**, 55 (2012)
30. N.V. Hong, M.T. Lan, N.T. Nhan, P.K. Hung, *Appl. Phys. Lett.* **102**, 191908 (2013)
31. I. Saika-Voivod, F. Sciortino, P.H. Poole, *Phys. Rev. E* **63**, 011202 (2000)